Differential-tilt technique for saturation-resistant profiling of atmospheric turbulence

Matthew R. Whiteley and Donald C. Washburn

Air Force Research Laboratory, Directed Energy Directorate,
3550 Aberdeen Avenue SE, Kirtland Air Force Base, New Mexico 87117-5776

ABSTRACT

A technique for profiling of C_n^2 over an atmospheric propagation path is proposed, developed and analyzed. The technique employs differential-tilt measurements to arrive at statistics which have unique weighting functions over the propagation path. These weighting functions are computed theoretically and used to derive a reconstructor matrix for C_n^2 values throughout the path to be applied to an appropriate set of differential-tilt statistics. A candidate optical system is presented, and the performance of the profile reconstructor is analyzed. This study indicates that the relative error in the C_n^2 estimates is approximately 5%. The relative error in estimating key atmospheric parameters such as the Fried parameter, isoplanatic angle, and the Rytov parameter from the reconstructed profiles is approximately 3%. The noise gain for estimating atmospheric parameters is less than 0.2 for all parameters considered.

Keywords: differential tilt, turbulence profiling, atmospheric characterization

1 INTRODUCTION

Compensation of atmospheric turbulence using adaptive-optics (AO) technology holds great promise for improving resolution of ground-based telescopes [1] and for improving target-plane energy density in laser weapon applications such as the Airborne Laser (ABL) [2, 3]. Optical resolution through the atmosphere with no compensation is governed by the relative aperture D/r_0, where D is the aperture diameter and r_0 is the atmospheric coherence diameter or Fried parameter [4]. Closed-loop performance of an AO system also depends upon D/r_0, but can be affected by turbulence characteristics such as the Rytov parameter ($\mathcal{R}$) [5] and isoplanatic angle (θ_0) [6]. The quantity D/r_0 indicates effects on the closed-loop system due to near-field turbulence, $\mathcal{R}$ indicates effects due to mid-path turbulence, and θ_0 indicates the effects of turbulence in the far-field. In general, it is necessary to know C_n^2 values along the propagation path at least at course resolution (or a sufficient set of atmospheric parameters) to assess closed-loop system performance [3].

Measurement of C_n^2 along a propagation path or as a function of altitude is often referred to as "turbulence profiling." Turbulence profiling is often conducted for the purpose of studying atmospheric phenomenology. In this case, high resolution profiles are required in order to address relevant phenomena. These types of studies have been effectively carried out using a profiling radar [7, 8, 9]. High-resolution studies have also been made using anemometry devices [2]. Integrated-turbulence profiling techniques are used when radar or in-situ techniques are impractical. In contrast to the radar or in-situ methods, integrated-turbulence profiling measurements tend to be low resolution. An example of this type of profiling is the Scintillation Detection and Ranging (SCIDAR) technique [10, 11]. A related technique for low-resolution profiling using pupil-plane irradiance imagery has also been proposed and tested by Holmes [3]. These low-resolution profiling

techniques are ideally suited for AO performance evaluation by use of theoretical analysis or wave-optics simulation.

In this paper, we introduce a new class of integrated-turbulence profiling techniques suitable for closed-loop AO performance analysis. The specific technique we discuss is built on a process known as the *difference of differential-tilt variance* (DDTV). The DDTV technique has many desirable properties, and has been shown to be effective for challenging atmospheric characterization problems [12]. Like the irradiance-based techniques discussed above, this technique produces relatively low resolution C_n^2 profiles as compared with radar or in-situ techniques. Unlike the irradiance-based techniques, this technique relies on phase-related quantities. Since differential-tilt measurements are phase-related, conventional propagation theory may be employed for analysis purposes even for strong extended-turbulence atmospheric paths. In this scenario, the variance of irradiance saturates (also called the *saturation regime* [13]) and there is no valid theoretical construct for treating irradiance statistics (i.e. variance, covariance). Thus, irradiance-based techniques are of limited utility in the saturation regime and not generally suitable for profiling over long nearly-horizontal paths with strong turbulence.

The technique we propose requires having a 2 receive apertures and an accompanying focal-plane camera on one end of the propagation path and 3 point source beacons on the other end of the path. Each aperture receives light from each of the point sources, leading to spot centroid measurements on the focal plane which form the fundamental data for the technique. An ensemble of fundamental data is collected, and then processed to form a collection of DDTV quantities. The particular DDTV quantities are selected a priori based on the uniqueness of their associated theoretical path-weighting function. For a given set of DDTV quantities determined from the data, a profile reconstructor matrix can be computed using theoretical analysis. When applied to the DDTV quantities, the output is a vector of C_n^2 values over the propagation path. Thus, the profile reconstructor is a linear operator on measurements made with the proposed apparatus.

The remainder of this paper is structured as follows. In Section 2, we discuss the theory and analysis supporting the differential-tilt profiling technique. Properties of the DDTV quantities are discussed, theoretical expressions for the associated path weighting functions are developed, and the form of the profile reconstructor matrix is derived. In Section 3 we give an example of how to determine the applicable set of DDTV quantities for a simple system configuration. We then present the results of performance testing for the proposed apparatus, demonstrating that this system provides an accurate and practical device for the C_n^2 profiling application. We draw conclusions in Section 4.

2 THEORY AND ANALYSIS

2.1 Properties of DDTV Measurements

To begin the analysis supporting this turbulence-profiling technique, we will first discuss the properties of a measurement process known as the *difference of differential-tilt variance* (DDTV), a technique introduced in Reference [12]. This process requires the measurement of two separate differential-tilt variances. We shall refer to these two differential-tilt variances as the *primary* and *secondary* variances. For each type of differential-tilt variance, there are fundamental measurements associated with each of two apertures, which we refer to as *aperture 1* and *aperture 2*. The fundamental measurements are centroids obtained on the focal plane associated with the two apertures. Aperture 1 and aperture 2 are in general separated physically, and are used to observe either a single point source or two individual point sources.

In this analysis, we designate the fundamental measurements associated with the two apertures for

the primary differential-tilt variance as d_{1p} and d_{2p}. Likewise, the fundamental measurements associated with the two apertures for the secondary differential-tilt variance are designated d_{1s} and d_{2s}. Using these measurements, the DDTV is designated σ_δ^2, and defined explicitly as:

$$\sigma_\delta^2 \equiv \left\langle (d_{1p} - d_{2p})^2 \right\rangle - \left\langle (d_{1s} - d_{2s})^2 \right\rangle, \tag{1}$$

where $\langle \cdot \rangle$ indicates the statistical expectation operation over an ensemble of turbulence realizations (a time history for ergodic turbulence assumptions). In the definition of Eq. (1), we have implicitly assumed that $\langle d_{1p} \rangle = \langle d_{2p} \rangle$ and $\langle d_{1s} \rangle = \langle d_{2s} \rangle$. Thus, any bias between the mean tilt of aperture 1 and the mean tilt of aperture 2 must be subtracted before applying Eq. (1) directly. It is worth noting here that Eq. (1) is a scalar equation to be applied to each component of the measured tilt vector. The analysis which follows will be carried out in a single axis of tilt parallel to the direction of the aperture separation vector.

The primary benefits of the DDTV technique are twofold. First, the DDTV technique is insensitive to contamination due to gimbal motion, a feature of all differential-tilt techniques [14, 15, 16]. Secondly, additive noise contributions to the differential-tilt variances are inherently canceled in the DDTV technique. To substantiate these claims, we consider a measurement model for tilt data from each aperture. In this measurement model, we express each tilt measurement as the sum three components; atmospheric, noise, and gimbal motion. Accordingly, the tilt data from each aperture is given by:

$$\begin{aligned} d_{1p} &= t_{1p} + n_{1p} + \theta_p, \\ d_{2p} &= t_{2p} + n_{2p} + \theta_p, \\ d_{1s} &= t_{1s} + n_{1s} + \theta_s, \\ d_{2s} &= t_{2s} + n_{2s} + \theta_s. \end{aligned} \tag{2}$$

In Eq. (2), t_{1p}, t_{2p} and t_{1s}, t_{2s} represent atmospheric tilt components of the measured data (in units of λ/D) from each aperture for primary and secondary differential-tilt statistics. Also, n_{1p}, n_{1s} and n_{2p}, n_{2s} represent the detector-noise-induced angle corresponding to each fundamental measurement. The contribution of gimbal motion to the measured tilt on each aperture is given by θ_p and θ_s, indicating that aperture 1 and aperture 2 are mounted on the same gimbal (gimbal motion contributes the same tilt to each aperture).

From the definition of σ_δ^2 in Eq. (1) and the model for the tilt data given in Eq. (2) it follows that:

$$\begin{aligned} \sigma_\delta^2 &= \left\langle (t_{1p} - t_{2p} + n_{1p} - n_{2p})^2 \right\rangle - \left\langle (t_{1s} - t_{2s} + n_{1s} - n_{2s})^2 \right\rangle \\ &= \left\langle t_{1p}^2 \right\rangle + \left\langle t_{2p}^2 \right\rangle - 2 \left\langle t_{1p} t_{2p} \right\rangle + \left\langle n_{1p}^2 \right\rangle + \left\langle n_{2p}^2 \right\rangle - 2 \left\langle n_{1p} n_{2p} \right\rangle \\ &\quad - \left\langle t_{1s}^2 \right\rangle - \left\langle t_{2s}^2 \right\rangle + 2 \left\langle t_{1s} t_{2s} \right\rangle - \left\langle n_{1s}^2 \right\rangle - \left\langle n_{2s}^2 \right\rangle + 2 \left\langle n_{1s} n_{2s} \right\rangle \\ &= 2 \left(\left\langle t_{1s} t_{2s} \right\rangle - \left\langle t_{1p} t_{2p} \right\rangle \right). \end{aligned} \tag{3}$$

In the steps leading up to Eq. (3), the noise variances and covariances are assumed to be equal for the primary and secondary measurements. We also assume that n_{1p}, n_{2p} are uncorrelated with t_{1p}, t_{2p} and n_{1s}, n_{2s} are uncorrelated with t_{1s}, t_{2s}. The gimbal-motion contributions are canceled by the differencing of the tilt measurements for the common-gimbal apertures. Furthermore, the atmospheric tilt variances as well as the noise variances and covariances are canceled by the differencing of the differential-tilt variances. All that remains in the expression for σ_δ^2 is the difference of atmospheric tilt covariances for the primary and secondary propagation geometries.

2.2 Path-Weighting Functions for DDTV Measurements

According to Eq. (3), σ_δ^2 represents twice the difference of tilt covariance between the two apertures for the primary and secondary propagation geometries. To derive a path-weighting function for σ_δ^2, we must first

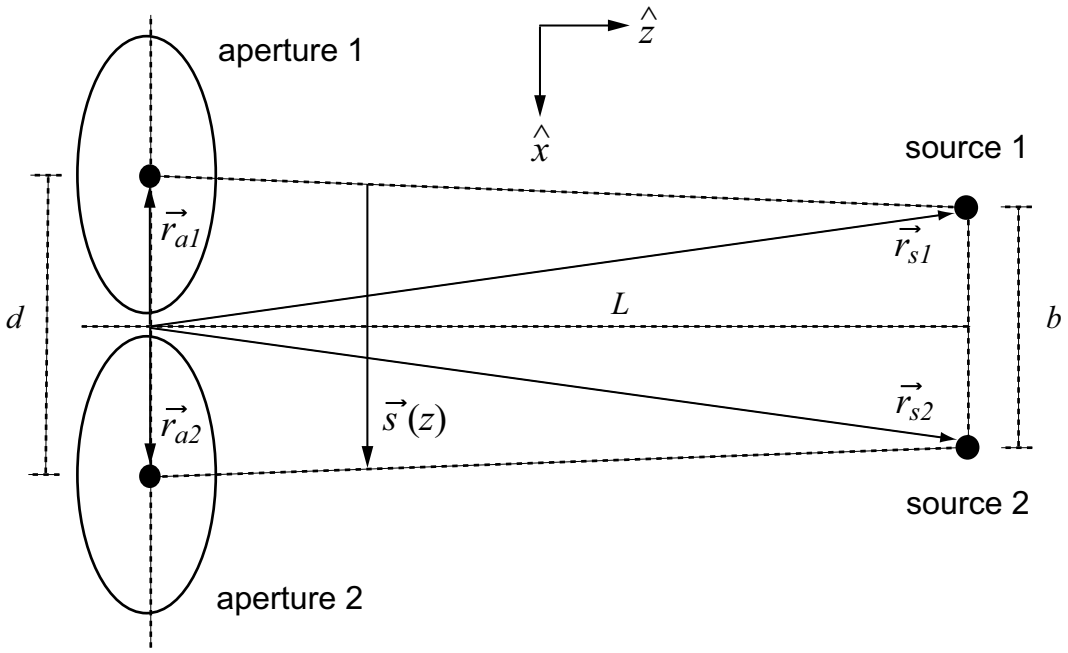

Figure 1: Analysis geometry for calculating the tilt covariance between apertures separated by a distance d in the $\hat{x}$ direction for point sources separated by a distance b in the $\hat{x}$ direction.

consider the relation between the tilt covariance and turbulence parameters for an arbitrary configuration of apertures and sources. This calculation has been performed previously for Zernike coefficients of arbitrary order, with arbitrarily-positioned apertures and sources [17, 18, 19]. To employ the results of these analyses here, we consider the geometry shown in Figure 1. This figure shows two apertures separated by a distance d in the $\hat{x}$ direction. These apertures receive light from two point sources separated by a distance b in the $\hat{x}$ direction. This geometry is general enough to model all possible differential-tilt configurations. The distances d and b may be set to zero when considering differential tilts with coincident (the same) apertures or sources.

For two apertures (diameter D) separated in the $\hat{x}$ direction assuming a finite outer scale for turbulence L_0, the covariance of the Zernike x-tilt coefficients for the two apertures, designated a_1 and a_2 is given by [17]:

$$\begin{aligned}\langle a_1 a_2 \rangle &= 2^{1/3}\sqrt{3}\,\Gamma(8/3)\left(\frac{2\pi}{\lambda}\right)^2 D^{5/3}\int_0^L \mathrm{d}z\; C_n^2(z)(1-z/L)^{-2} \\ &\quad\times\int_0^\infty \frac{\mathrm{d}x}{x}(x^2+x_0^2)^{-11/6}J_2^2[(1-z/L)x]\left\{J_0\left[\frac{2s(z)}{D}x\right]-J_2\left[\frac{2s(z)}{D}x\right]\right\},\end{aligned} \tag{4}$$

where λ is the wavelength, L is the propagation distance, C_n^2 is the index of refraction structure constant, $x_0 = \pi D/L_0$, and $s(z)$ is the magnitude of $\vec{s}(z)$ shown in Figure 1:

$$\vec{s}(z) = (1-z/L)(\vec{r}_{a_2}-\vec{r}_{a_1})+(z/L)(\vec{r}_{s_2}-\vec{r}_{s_1}), \tag{5}$$

$$s(z) = d(1-z/L)+b(z/L). \tag{6}$$

Notice that since the aperture and source separations are in the $\hat{x}$ direction, $\vec{s}(z)$ is always parallel to $\hat{x}$. As

defined, the Zernike tilt coefficient a is related to an angular tilt t (in units of λ/D) by $a = (2/\pi)t$.

The physical configurations we wish to consider involve small separations of the apertures and sources. In these cases, outer scale effects will be negligible. Thus, for $x_0 \to 0$, Eq. (4) may be written as:

$$\langle a_1 a_2 \rangle = 16\sqrt{3}\,\Gamma(8/3)\left(\frac{2\pi}{\lambda}\right)^2 D^{5/3} L \int_0^1 \mathrm{d}\xi\; C_n^2(\xi L)\,\frac{[\alpha(\xi)]^{11/3}}{(1-\xi)^{-2}} \int_0^\infty \frac{\mathrm{d}\gamma}{\gamma}\gamma^{-11/3} J_2^2[\beta(\xi)\gamma]\Big\{J_0(\gamma) - J_2(\gamma)\Big\}, \quad (7)$$

where $\xi = z/L$ and $\alpha(\xi)$, $\beta(\xi)$ are dimensionless parameters given by:

$$\alpha(\xi) = \frac{s(\xi)}{D}, \quad (8)$$

$$\beta(\xi) = \frac{1-\xi}{2\alpha(\xi)}. \quad (9)$$

From Eq. (6) and Eq. (8) we note that $\langle a_1 a_2 \rangle$ for a given $C_n^2(z)$ depends only upon the normalized aperture separation d/D and the normalized source separation b/D. If we treat all factors multiplying C_n^2 within the integral over ξ as a weighting function $W(\xi)$, then Eq. (7) may be rewritten as:

$$\langle a_1 a_2 \rangle = 16\sqrt{3}\,\Gamma(8/3)\left(\frac{2\pi}{\lambda}\right)^2 D^{5/3} L \int_0^1 \mathrm{d}\xi\; C_n^2(\xi L)\; W(\xi), \quad (10)$$

where $W(\xi)$ is defined as:

$$W(\xi) \equiv \frac{[\alpha(\xi)]^{11/3}}{(1-\xi)^{-2}} \int_0^\infty \frac{\mathrm{d}\gamma}{\gamma}\gamma^{-11/3} J_2^2[\beta(\xi)\gamma]\Big\{J_0(\gamma) - J_2(\gamma)\Big\}. \quad (11)$$

The integral over γ may be evaluated in closed form. The value of the integral depends upon the value of the parameter $\beta(\xi)$ as follows:

For $[\beta(\xi)]^2 < 1/4$:

$$W(\xi) = 2^{-14/3}(1-\xi)^{5/3}\left[\begin{array}{l} 2^{-17/3}[\beta(\xi)]^{1/3}\dfrac{\Gamma(1/6)}{\Gamma(5/6)}\;{}_3F_2\left\{1/6, 1/6, 5/2; 3, 5; [2\beta(\xi)]^2\right\} \\ \\ -2^{-17/3}[\beta(\xi)]^{1/3}\dfrac{\Gamma(7/6)}{\Gamma(11/6)}\;{}_3F_2\left\{-5/6, 7/6, 5/2; 3, 5; [2\beta(\xi)]^2\right\} \end{array}\right] \quad (12)$$

For $[\beta(\xi)]^2 \geq 1/4$:

$$W(\xi) = 2^{-14/3}(1-\xi)^{5/3}\left[\begin{array}{l} \dfrac{\Gamma(1/6)\Gamma(7/3)\;{}_3F_2\left\{-23/6, 11/6, 1/6; -4/3, 1; [2\beta(\xi)]^{-2}\right\}}{\sqrt{\pi}\Gamma(17/6)\Gamma(29/6)} \\ \\ +\dfrac{\Gamma(-7/3)\;{}_3F_2\left\{-3/2, 1/2, 5/2; 10/3, 10/3; [2\beta(\xi)]^{-2}\right\}}{2^{14/3}\pi\Gamma(10/3)[\beta(\xi)]^{14/3}} \\ \\ -\dfrac{\Gamma(7/6)\Gamma(4/3)\;{}_3F_2\left\{-17/6, -5/6, 7/6; -1/3, 3; [2\beta(\xi)]^{-2}\right\}}{2^3\sqrt{\pi}\Gamma(11/6)\Gamma(23/6)[\beta(\xi)]^2} \\ \\ -\dfrac{\Gamma(-4/3)\;{}_3F_2\left\{-3/2, 1/2, 5/2; 7/3, 13/3; [2\beta(\xi)]^{-2}\right\}}{2^{14/3}\pi\Gamma(13/3)[\beta(\xi)]^{14/3}} \end{array}\right] \quad (13)$$

Throughout the remainder of this paper, we will investigate weighting functions of C_n^2 corresponding to different optical configurations. To facilitate our discussion, we have chosen to work with normalized weighting functions, that is, weighting functions whose integral value over the propagation path is 1. In normalized form, Eq. (10) is written as:

$$\langle a_1 a_2 \rangle = 16\sqrt{3}\,\Gamma(8/3)\left(\frac{2\pi}{\lambda}\right)^2 D^{5/3} L\, W_0 \int_0^1 \mathrm{d}\xi\ C_n^2(\xi L)\ w(\xi), \tag{14}$$

where

$$w(\xi) = \frac{W(\xi)}{W_0}, \tag{15}$$

$$W_0 \equiv \int_0^1 \mathrm{d}\xi\, W(\xi). \tag{16}$$

When normalized in this fashion, $w(\xi)$ in Eq. (14) is analogous to a probability density for the tilt covariance over the propagation path. The integral of $w(\xi)$ over some interval $\Delta\xi$ gives the probability that the turbulence strength within $\Delta\xi$ contributes to the tilt covariance.

Recall from Eq. (3) that σ_δ^2 is given as 2 times the difference of the tilt covariances for the primary and secondary propagation geometries. Using Eq. (14), we see that σ_δ^2 is given by:

$$\begin{aligned}
\sigma_\delta^2 &= 2\left(\langle t_{1s} t_{2s}\rangle - \langle t_{1p} t_{2p}\rangle\right) \\
&= \frac{8}{\pi^2}\left(\langle a_{1s} a_{2s}\rangle - \langle a_{1p} a_{2p}\rangle\right) \\
&= \frac{128\sqrt{3}\,\Gamma(8/3)}{\pi^2}\left(\frac{2\pi}{\lambda}\right)^2 D^{5/3} L \int_0^1 \mathrm{d}\xi\ C_n^2(\xi L)\ \left[W_{0s} w_s(\xi) - W_{0p} w_p(\xi)\right] \\
&= \frac{128\sqrt{3}\,\Gamma(8/3)}{\pi^2}\left(\frac{2\pi}{\lambda}\right)^2 D^{5/3} L \left(W_{0s} - W_{0p}\right) \int_0^1 \mathrm{d}\xi\ C_n^2(\xi L)\ w_\delta(\xi),
\end{aligned} \tag{17}$$

where W_{0s}, $w_s(\xi)$ and W_{0p}, $w_p(\xi)$ are the normalization constant and normalized weighting function for the secondary and primary geometries, respectively. The factor of $4/\pi^2$ arising in the second step represents a conversion of Zernike-tilt variance in units of rad^2 to angular variance in units of $(\lambda/D)^2$. Notice that the weighting function for the difference of the tilt covariances is the difference of the weighting functions of each covariance. In Eq. (17), we have chosen to normalize the weighting function for σ_δ^2 as follows:

$$\begin{aligned}
w_\delta(\xi) &\equiv \frac{W_{0s} w_s(\xi) - W_{0p} w_p(\xi)}{\int_0^1 \mathrm{d}\xi\, W_{0s} w_s(\xi) - W_{0p} w_p(\xi)} \\
&= \frac{W_{0s} w_s(\xi) - W_{0p} w_p(\xi)}{W_{0s}\int_0^1 \mathrm{d}\xi\, w_s(\xi) - W_{0p}\int_0^1 \mathrm{d}\xi\, w_p(\xi)} \\
&= \frac{W_{0s} w_s(\xi) - W_{0p} w_p(\xi)}{W_{0s} - W_{0p}},
\end{aligned} \tag{18}$$

where the last step in the equation above follows from the fact that w_s and w_p are normalized.

2.3 Derivation of the Turbulence-Profile Reconstructor

The main result to be taken from Subsection 2.2 is that any DDTV statistic generated using an arbitrary array of apertures with an arbitrary array of point sources can be expressed as a weighted integral of $C_n^2(z)$.

Furthermore, DDTV path weighting functions can be evaluated in closed-form given the normalized aperture separation and the normalized source separation for the primary and secondary configurations. For a given array of apertures and point sources, suppose we consider M-DDTV measurements indexed by the subscript k. For each DDTV measurement, from Eq. (17) we know that for $k = 1, 2, \ldots, M$:

$$\sigma^2_{\delta\,k} = \frac{128\sqrt{3}\,\Gamma(8/3)}{\pi^2}\left(\frac{2\pi}{\lambda}\right)^2 D^{5/3} L\, W_{0k} \int_0^1 \mathrm{d}\xi\ C_n^2(\xi L)\ w_{\delta k}(\xi), \tag{19}$$

where $w_{\delta k}(\xi)$ is the normalized path-weighting function for $\sigma^2_{\delta\,k}$ and $W_{0k} = (W_{0s} - W_{0p})_k$. From Eq. (19) we may say that:

$$m_k = \int_0^1 \mathrm{d}\xi\ C_n^2(\xi L)\ w_{\delta k}(\xi), \tag{20}$$

where m_k is the kth normalized DDTV measurement given by:

$$m_k = \frac{\sigma^2_{\delta\,k}}{\frac{128\sqrt{3}\,\Gamma(8/3)}{\pi^2}\left(\frac{2\pi}{\lambda}\right)^2 D^{5/3} L\, W_{0k}}. \tag{21}$$

Now, suppose that $C_n^2(\xi L)$ is well modeled by N partitions of nearly-uniform turbulence strength such that:

$$C_n^2(\xi L) = \sum_{i=1}^{N} C_{n\,i}^2\, \mathrm{rect}\left(\frac{\xi - \xi_i}{l_i}\right), \tag{22}$$

where $C_{n\,i}^2$ is the uniform turbulence strength over partition i, ξ_i is the normalized position of the center of the of the ith partition of normalized width l_i (i.e., $\sum_{i=1}^{N} l_i = 1$). With the model for $C_n^2(z)$ given in Eq. (22), we may use Eq. (20) to write:

$$\begin{aligned} m_k &= \int_0^1 \mathrm{d}\xi \sum_{i=1}^{N} C_{n\,i}^2\, \mathrm{rect}\left(\frac{\xi - \xi_i}{l_i}\right) w_{\delta k}(\xi) \\ &= \sum_{i=1}^{N} C_{n\,i}^2 \int_0^1 \mathrm{d}\xi\, \mathrm{rect}\left(\frac{\xi - \xi_i}{l_i}\right) w_{\delta k}(\xi) \\ &= \sum_{i=1}^{N} C_{n\,i}^2 \int_{\xi_i - l_i/2}^{\xi_i + l_i/2} \mathrm{d}\xi\, w_{\delta k}(\xi) \\ &= \sum_{i=1}^{N} C_{n\,i}^2\, p_{ki}, \end{aligned} \tag{23}$$

where p_{ki} is integral of the kth weighting function over the ith path partition:

$$p_{ki} = \int_{\xi_i - l_i/2}^{\xi_i + l_i/2} \mathrm{d}\xi\, w_{\delta k}(\xi). \tag{24}$$

At this point, we recognize that Eq. (23) represents a system of M equations with N unknowns which may be written compactly in vector-matrix form using the following notation:

$$\mathbf{m} = \begin{bmatrix} m_1 \\ m_2 \\ \vdots \\ m_M \end{bmatrix} \qquad \mathbf{P} = \begin{bmatrix} p_{11} & p_{12} & \cdots & p_{1N} \\ p_{21} & p_{22} & & \vdots \\ \vdots & & \ddots & \vdots \\ p_{M1} & \cdots & \cdots & p_{MN} \end{bmatrix} \qquad \mathbf{c} = \begin{bmatrix} C_{n1}^2 \\ C_{n2}^2 \\ \vdots \\ C_{nN}^2 \end{bmatrix}. \tag{25}$$

Thus, the system of equations specified in Eq. (23) may be rewritten as:

$$\mathbf{m} = \mathbf{P}\mathbf{c}. \tag{26}$$

Eq. (26) expresses the transformation of a set of C_n^2 values over the propagation path (a turbulence profile) to the normalized DDTV measurements each of which should represent a unique moment of the turbulence profile.

The goal of any turbulence profiling technique is a problem inverse to the set of equations indicated in Eq. (26); that is, given a set of normalized DDTV measurements, determine the vector of C_n^2 values from which those measurements were derived. If $\mathbf{P}$ were an invertible matrix, then the solution to Eq. (26) would be $\mathbf{c} = \mathbf{P}^{-1}\mathbf{m}$. However, $\mathbf{P}$ is generally not invertible, and we instead seek an optimal solution for Eq. (26). The least-squares estimate $\hat{\mathbf{c}}$ for $\mathbf{c}$ is a common optimal solution [20] given by:

$$\hat{\mathbf{c}} = \mathbf{H}\mathbf{m}, \tag{27}$$

where $\mathbf{H}$ is the well-known pseudo-inverse [21] of $\mathbf{P}$ given by:

$$\mathbf{H} = (\mathbf{P}^T\mathbf{P})^{-1}\mathbf{P}^T. \tag{28}$$

We will refer to $\mathbf{H}$ as the turbulence profile "reconstructor." Given a set of M normalized DDTV measurements, $\mathbf{H}$ will be used to reconstruct N partitions of C_n^2 over the propagation path. The profile reconstructor is computed directly from the $\mathbf{P}$ matrix, whose elements are derived by integrating the analytic weighting functions of the appropriate DDTV measurements over the desired path partitions.

3 RESULTS

Section 2 and its constituent subsections provide the full theoretical structure required for developing and analyzing a turbulence profiling technique using the DDTV method. For a given set of apertures and point sources, the weighting functions for DDTV statistics under consideration can be calculated and integrated properly to derive a reconstructor matrix for C_n^2 over a set of path partitions. In this section, we provide a simple example of how to determine the set of DDTV statistics to be included in the measurement vector. We also consider a practical profiling apparatus and assess its performance against random turbulence profiles.

3.1 Determining the DDTV Measurement Set: An Example

We now provide an example of how to determine the set of DDTV statistics to be included in the measurement vector for the profile reconstructor. The example is given for a simple array of apertures and point sources, but the methodology presented can be applied to more complex configurations to arrive at an applicable profile reconstructor. The logic described here has been implemented in computer code and applied to develop the turbulence profiler described in Subsection 3.2.

In particular, we will consider the unique DDTV statistics arising from an apparatus comprised of two apertures located at $x = 0, 1$ and $z = 0$. These apertures receive light from two point sources located at $x = 0, 1$ and $z = L$. Each aperture receives light from each point source. Thus, a centroid calculation can be made on the focal plane associated with each aperture from each point source. The matrix on the left-hand side of Table 1 shows the fundamental data elements (centroids) derived from the 2-aperture/2-source system. The matrix on the right-hand side of Table 1 shows the unique differential-tilt variances that can be computed using these fundamental data elements.

	source location	
aperture location	0	1
0	d_{00}	d_{01}
1	d_{10}	d_{11}

	d_{00}	d_{01}	d_{10}	d_{11}
d_{00}	****	$\langle(d_{00}-d_{01})^2\rangle$	$\langle(d_{00}-d_{10})^2\rangle$	$\langle(d_{00}-d_{11})^2\rangle$
d_{01}	****	****	$\langle(d_{01}-d_{10})^2\rangle$	$\langle(d_{01}-d_{11})^2\rangle$
d_{10}	****	****	****	$\langle(d_{10}-d_{11})^2\rangle$
d_{11}	****	****	****	****

Table 1: Data specification for unique differential-tilt variances using apertures located at $x = 0, 1$ and point sources located at $x = 0, 1$. Each fundamental data element is generated by each aperture receiving light from each point source (left). Diagonal elements for the matrix of differential-tilt variances (right) using these fundamental data elements are 0. Matrix elements to the left of the diagonal are the same as the elements to the right of the diagonal.

While each of the differential-tilt variances shown in Table 1 are unique, not all will result in unique contributions to the weighting functions associated with DDTV statistics. Remember that the DDTV path weighting is the difference of tilt covariance path weighting functions. The tilt covariance weighting functions are determined by the normalized aperture separation d/D and the normalized source separation b/D. By examining the value of these parameters for each of the differential-tilt variances indicated in Table 1, we can determine which of these are worthy of further consideration. This process is shown graphically in Figure 2. These diagrams show the optical propagation geometry for each of the 6 differential-tilt variances indicated in Table 1 (ordering each by going across the rows). Notice that configurations 5 and 6 have the same set of aperture and source separation parameters as configurations 2 and 1, respectively.

DDTV designation	specification
$\sigma^2_{\delta 1}$	$\langle(d_{00}-d_{01})^2\rangle - \langle(d_{00}-d_{10})^2\rangle$
$\sigma^2_{\delta 2}$	$\langle(d_{00}-d_{01})^2\rangle - \langle(d_{00}-d_{11})^2\rangle$
$\sigma^2_{\delta 3}$	$\langle(d_{00}-d_{01})^2\rangle - \langle(d_{01}-d_{10})^2\rangle$
$\sigma^2_{\delta 4}$	$\langle(d_{00}-d_{10})^2\rangle - \langle(d_{00}-d_{11})^2\rangle$
$\sigma^2_{\delta 5}$	$\langle(d_{00}-d_{10})^2\rangle - \langle(d_{01}-d_{10})^2\rangle$
$\sigma^2_{\delta 6}$	$\langle(d_{00}-d_{11})^2\rangle - \langle(d_{01}-d_{10})^2\rangle$

Table 2: Specification for the 6 DDTV statistics resulting in unique path-weighting functions from an apparatus with apertures located at $x = 0, 1; z = 0$ and sources located at $x = 0, 1; z = L$

Eliminating the two configurations giving duplicate covariance weighting, there are 4 differential-tilt variances which can be used to form DDTV measurements with unique path-weighting functions. The specification for each of the 6 such DDTV statistics is given in Table 2. These path weighting functions (properly normalized) are depicted in Figure 3. These plots indicate that even for a modest array of apertures and point sources, the unique DDTV statistics which result have path weighting functions with vastly different characteristics. Some give more weighting to the aperture-end of the path, while others accentuate the mid-path. These plots also indicate that none of the DDTV measurements are well-weighted at the source-end of the path. This is a inherent characteristic of differential-tilt measurements from point sources.

To obtain reliable profiling of turbulence strength near $z = L$, we will consider using a bi-directional system. To create such a system, apparatus at either end of the path is duplicated on the other. For the example given in this subsection, this results in a set of DDTV weighting functions similar to those shown in Figure 3, but flipped left-to-right. For a bi-directional system with M-DDTV measurements coming from each end of the path, the measurement vector has $2M$ elements, and the associated weighting functions for $k > M$ are given by:

$$w_{\delta k}(\xi) = w_{\delta k-M}(1-\xi). \tag{29}$$

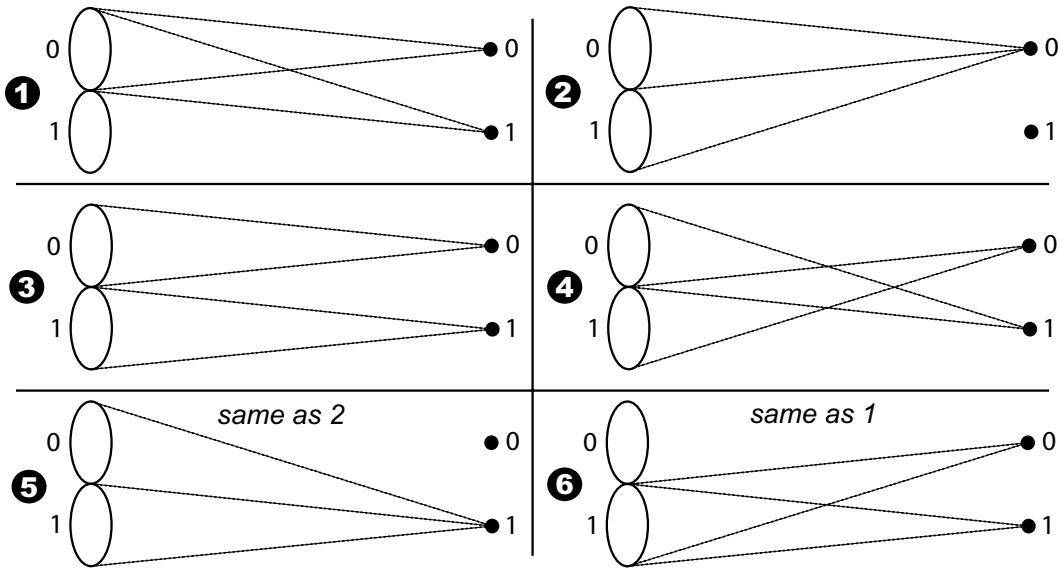

Figure 2: Collection of all possible differential-tilt variance configurations obtained with apertures located at $x = 0, 1$ and point sources located at $x = 0, 1$. Two configurations do not yield unique tilt-covariance weighting functions.

3.2 Performance of the Proposed Profiling Apparatus

Having detailed the process of determining DDTV statistics to be included in the measurement vector for a simple optical configuration, we now consider a practical apparatus for turbulence profiling. This apparatus is considered to be "practical" in the sense that it requires a modest investment in hardware and exhibits desirable reconstructor performance. The proposed optical configuration is shown in Figure 4. As this diagram indicates, the proposed configuration features 2 apertures at $z = 0$ and 3 point sources at the other end of the path ($z = L$). The system is bi-directional, so similar hardware is located on either end of the propagation path. The system aperture centers are separated by D, and the point source separations are D and $2D$. By spacing the point sources unevenly, we are allowing for a greater number of unique DDTV statistics to be generated by the configuration.

Following the line of reasoning outlined in Subsection 3.1, it was determined that each end of the system shown in Figure 4 yields 45 DDTV measurements, each of which have a unique weighting function. Thus, the number of elements in the measurement vector is 90 for the bi-directional system. To compute the transformation matrix $\mathbf{P}$, we assumed a turbulence profile with 10 partitions, resulting in a $\mathbf{P}$ matrix which is of size 90x10. The reconstructor matrix $\mathbf{H}$ was computed from $\mathbf{P}$ using Eq. (28). To test this reconstructor, random turbulence profiles were generated with 10 partitions across the path. The C_n^2 values over the 10 partitions were computed according to:

$$C_{ni}^2 = C_0 \exp(x_i), \tag{30}$$

where x_i are random numbers drawn from a normal distribution with 0 mean and unit variance (C_{ni}^2 values are log-normal). The constant C_0 was set to 5.0×10^{-17} m$^{-2/3}$.

An ensemble of 1,000 random turbulence profiles was generated, and the appropriate moments of each distribution were computed to form the measurement vector $\mathbf{m}$. The turbulence profile estimate vector $\hat{\mathbf{c}}$ was

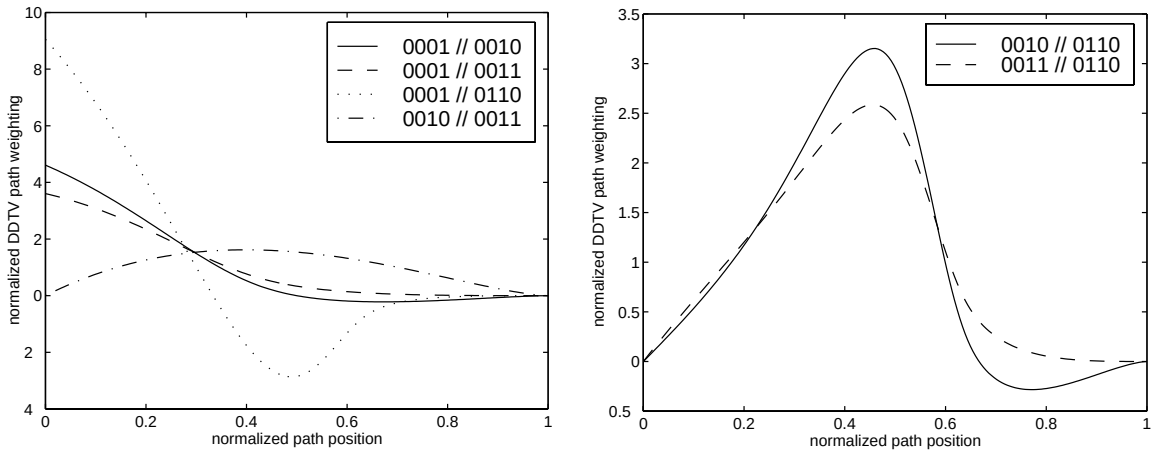

Figure 3: Path-weighting functions for the 6 DDTV measurements indicated in Table 2. Legend represents coded specification of DDTV measurement, e.g. "0001 // 0010" represents $\left\langle (d_{00} - d_{01})^2 \right\rangle - \left\langle (d_{00} - d_{10})^2 \right\rangle$

computed for each of the random profiles by applying the reconstructor matrix $\mathbf{H}$ to $\mathbf{m}$ according to Eq. (27). A sampling of the reconstruction results for the ensemble of turbulence profiles is shown in Figure 5(a). The relative error for the ensemble of reconstructed profiles is shown in Figure 5(b). This plots illustrates that the relative error in the reconstructed profile is generally quite small over most of the propagation path. The mean relative error is approximately 5%, whereas the median relative error is approximately 3%. Even the relative error for 85% of the distribution is less than 10% over the entire propagation path.

While the relative error characteristics shown in Figure 5(b) indicate that the proposed turbulence profiler will perform quite well, it is perhaps more instructive to consider how well the reconstructed profiles can be employed to determine key atmospheric parameters. Estimates of key atmospheric parameters like the Rytov parameter ($\mathcal{R}$), Fried parameter (r_0), isoplanatic angle (θ_0) may be used together to assess how well an adaptive-optics system might perform [3]. Using the ensemble of 1,000 random profiles and the reconstruction results associated with each of these profiles, the following atmospheric parameters were computed:

$$\text{Rytov parameter: } \mathcal{R} = 0.5631 \left(\frac{2\pi}{\lambda}\right)^{7/6} L^{11/6} \int_0^1 \mathrm{d}\xi \, C_n^2(\xi L) \, [\xi(1-\xi)]^{5/6} \tag{31}$$

$$\text{Fried parameter: } r_0 = \left[\frac{2.91}{6.88} \left(\frac{2\pi}{\lambda}\right)^2 L \int_0^1 \mathrm{d}\xi \, C_n^2(\xi L) \, (1-\xi)^{5/3}\right]^{-3/5} \tag{32}$$

$$\text{isoplanatic angle: } \theta_0 = \left[2.91 \left(\frac{2\pi}{\lambda}\right)^2 L^{8/3} \int_0^1 \mathrm{d}\xi \, C_n^2(\xi L) \, \xi^{5/3}\right]^{-3/5} \tag{33}$$

$$\text{integrated turbulence: } m_0 = \int_0^1 \mathrm{d}\xi \, C_n^2(\xi L), \tag{34}$$

where λ is the wavelength and L is the path length. For the purpose of this study, $\lambda = 1.0 \times 10^{-6}$m and $L = 5.0 \times 10^4$m were used in calculating the atmospheric parameters. Scatter plots of the atmospheric parameters computed for the reconstructed profiles versus the atmospheric parameters for the original profiles are shown in Figure 6(a). These plots show that the key atmospheric parameters values arising from the reconstructed profiles are indeed highly correlated with the atmospheric parameters of the original profiles. Figure 6(b) shows cumulative distribution curves for the relative error associated with each atmospheric parameter

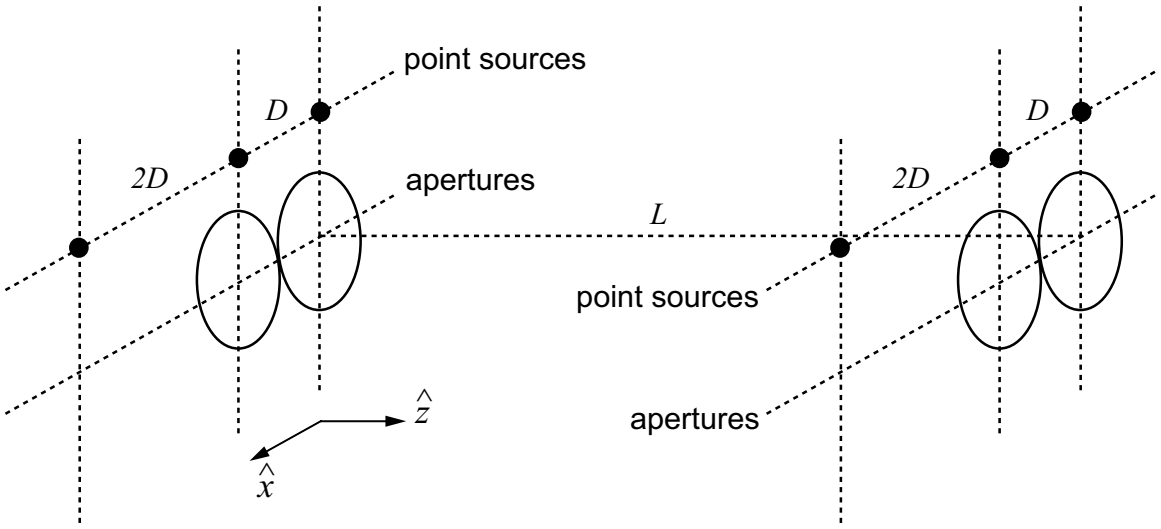

Figure 4: Optical configuration for the proposed profiling apparatus. Two apertures are separated in the $\hat{x}$ direction by the aperture diameter D. Three down range point sources are separated in the $\hat{x}$ direction by distances D and $2D$. An equivalent symmetric system is also located down range.

estimated from the reconstructed profiles. The relative error performance for r_0 and θ_0 is approximately the same, with all relative errors less than 2%. There are slightly larger errors associated with determining $\mathcal{R}$ and m_0 from the reconstructed profiles, but both have errors near 3%.

3.3 Reconstructor Noise Gain

The analysis in Subsection 3.2 illustrates that the proposed profiling apparatus is capable of accurately reconstructing C_n^2 values over the propagation path. Consequently, estimates of key atmospheric parameters are also accurately obtained. In this subsection, we address the precision of the profile reconstructor and the impact on estimates of atmospheric parameters.

Each of the expressions in Eq. (32) through Eq. (34) can be rewritten as a weighted integral of C_n^2 over the propagation path to define a generalized parameter value p given by:

$$\begin{aligned} p &= \frac{f(\lambda, L) \int_0^1 \mathrm{d}\xi \, C_n^2(\xi L) \, w_p(\xi)}{f(\lambda, L)} \\ &= \int_0^1 \mathrm{d}\xi \, C_n^2(\xi L) \, w_p(\xi), \end{aligned} \tag{35}$$

where $f(\lambda, L)$ is an arbitrary function for each parameter and $w_p(\xi)$ is a weighting function normalized such that $\int_0^1 \mathrm{d}\xi \, w_p(\xi) = 1$. For the partitioned turbulence profile given in Eq. (22), Eq. (35) can be written as:

$$p = \int_0^1 \mathrm{d}\xi \sum_{i=1}^{N} C_{ni}^2 \, \mathrm{rect}\left(\frac{\xi - \xi_i}{l_i}\right) w_p(\xi)$$

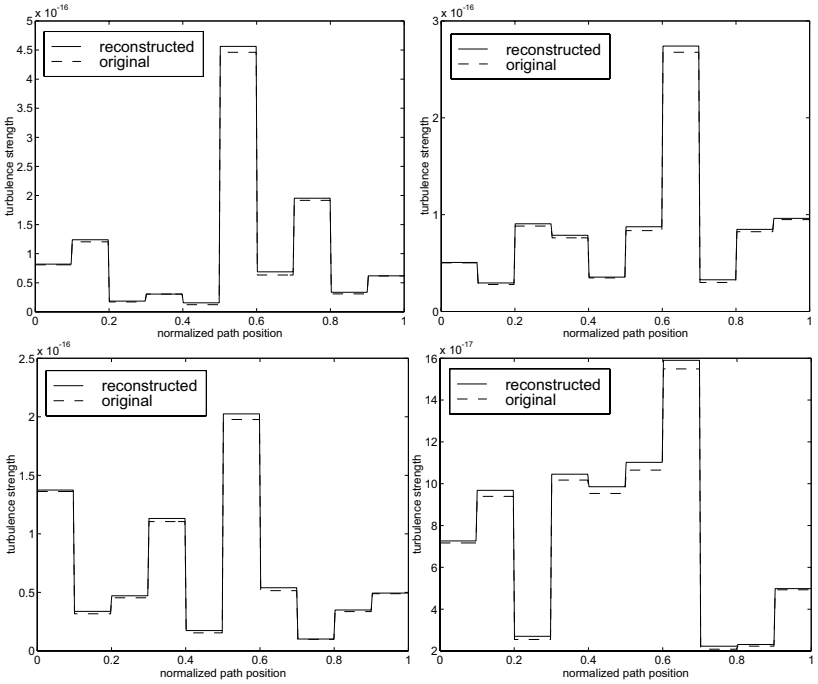

(a)

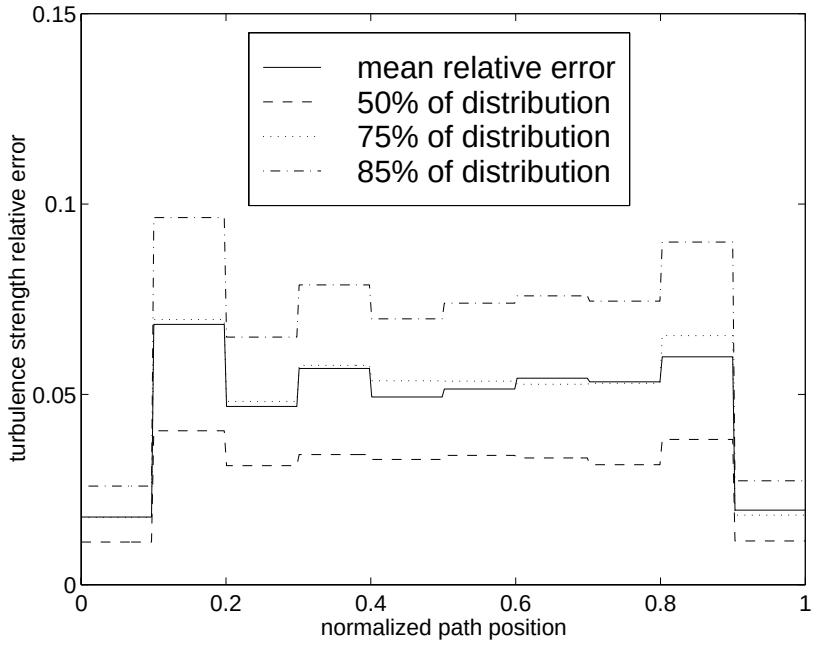

(b)

Figure 5: (a) Sampling of reconstructor performance for a bi-directional system employing two apertures and three point sources on each end of the propagation path. (b) Relative error in C_n^2 estimation for an ensemble of 1000 random turbulence profiles with 10 partitions across the path.

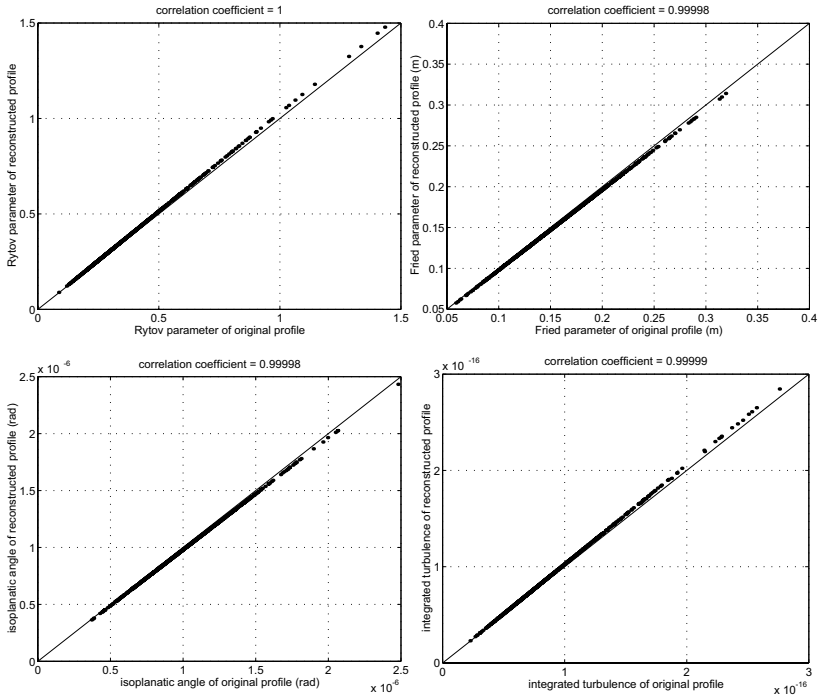

(a)

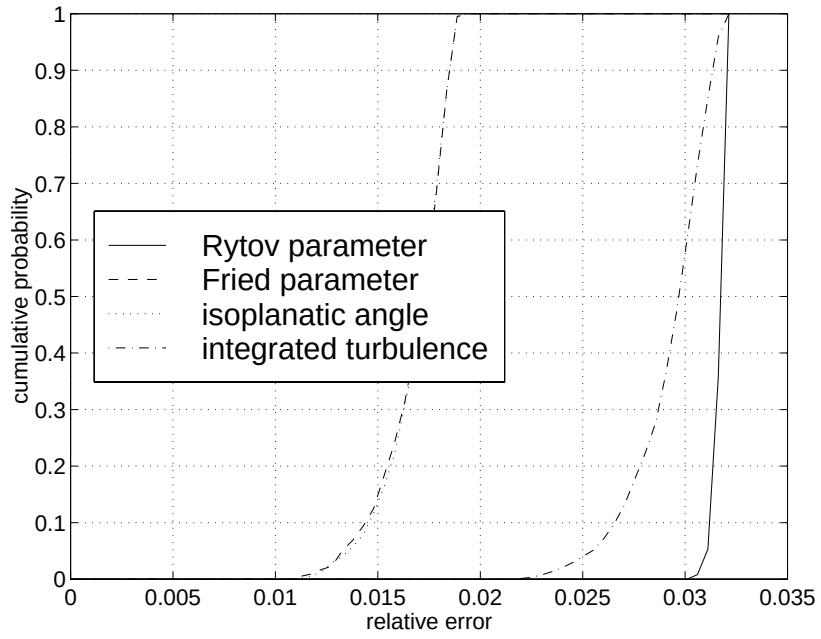

(b)

Figure 6: (a) Atmospheric parameters for each reconstructed profile versus atmospheric parameters for each of 1000 random turbulence profiles with 10 partitions across the propagation path. (b) Cumulative distribution functions of the relative error in atmospheric parameters calculated from reconstructed turbulence profiles.

$$
\begin{aligned}
p &= \sum_{i=1}^{N} C_{ni}^2 \int_0^1 \mathrm{d}\xi \, \mathrm{rect}\left(\frac{\xi - \xi_i}{l_i}\right) \, w_p(\xi) \\
p &= \sum_{i=1}^{N} C_{ni}^2 \int_{\xi_i - l_i/2}^{\xi_i + l_i/2} \mathrm{d}\xi \, w_p(\xi) \\
p &= \sum_{i=1}^{N} C_{ni}^2 \, A_i, \qquad (36)
\end{aligned}
$$

where A_i is integral of the parameter weighting function over the ith path partition:

$$
A_i = \int_{\xi_i - l_i/2}^{\xi_i + l_i/2} \mathrm{d}\xi \, w_p(\xi). \qquad (37)
$$

Thus, the generalized parameter value may be related to a vector $\mathbf{c}$ of C_n^2 values according to:

$$
p = \mathbf{A}\,\mathbf{c}, \qquad (38)
$$

where $\mathbf{A} = [A_1 \;\; A_2 \;\; \ldots \;\; A_N]$.

To address the precision of the profile reconstructor and the impact of this precision on the estimate $\hat{p}$ of the atmospheric parameter p, we first consider that $\hat{p} = \mathbf{A}\,\hat{\mathbf{c}}$. From Eq. (27), it therefore holds that $\hat{p} = \mathbf{A}\,\mathbf{H}\,\mathbf{m}$. Now, from this relationship, it follows that for a small change in $\mathbf{m}$, designated $\mathrm{d}\mathbf{m}$:

$$
\mathrm{d}\hat{p} = \mathbf{A}\,\mathbf{H}\,\mathrm{d}\mathbf{m}. \qquad (39)
$$

Given this relationship, we may then consider the mean-squared value of $\mathrm{d}\hat{p}$, designated here as $\sigma_{\hat{p}}^2$:

$$
\begin{aligned}
\sigma_{\hat{p}}^2 &= \left\langle \mathrm{d}\hat{p}^2 \right\rangle \\
&= \left\langle (\mathbf{A}\,\mathbf{H}\,\mathrm{d}\mathbf{m})(\mathbf{A}\,\mathbf{H}\,\mathrm{d}\mathbf{m})^T \right\rangle \\
&= \mathbf{A}\,\mathbf{H}\,\left\langle \mathrm{d}\mathbf{m}\,\mathrm{d}\mathbf{m}^T \right\rangle\,\mathbf{H}^T\,\mathbf{A}^T. \qquad (40)
\end{aligned}
$$

If we regard $\mathrm{d}\mathbf{m}$ as a noise term in the measurement vector, then it is reasonable to assume the elements of $\mathrm{d}\mathbf{m}$ are mutually uncorrelated. Furthermore, if each element has an equal variance σ_m^2, then we may say that:

$$
\left\langle \mathrm{d}\mathbf{m}\,\mathrm{d}\mathbf{m}^T \right\rangle = \sigma_m^2\,\mathbf{I} \qquad (41)
$$

Using this form for the covariance matrix of $\mathbf{m}$, and employing the fact that $\mathbf{H} = (\mathbf{P}^T\mathbf{P})^{-1}\mathbf{P}^T$, it follows that:

$$
\begin{aligned}
\sigma_{\hat{p}}^2 &= \mathbf{A}\,\mathbf{H}\,\sigma_m^2\,\mathbf{I}\,\mathbf{H}^T\,\mathbf{A}^T \\
&= \mathbf{A}\,(\mathbf{P}^T\mathbf{P})^{-1}\mathbf{P}^T\mathbf{P}(\mathbf{P}^T\mathbf{P})^{-1}\mathbf{A}^T\,\sigma_m^2 \\
&= \left[\mathbf{A}\,(\mathbf{P}^T\mathbf{P})^{-1}\mathbf{A}^T\right]\sigma_m^2 \qquad (42)
\end{aligned}
$$

For a measurement value m, we can use the relationship in Eq. (42) to write:

$$
\begin{aligned}
\frac{\sigma_{\hat{p}}^2}{p^2} &= \left[\mathbf{A}\,(\mathbf{P}^T\mathbf{P})^{-1}\mathbf{A}^T\right]\,\frac{m^2}{p^2}\,\frac{\sigma_m^2}{m^2} \\
\frac{\sigma_{\hat{p}}}{p} &= \left[\sqrt{\mathbf{A}\,(\mathbf{P}^T\mathbf{P})^{-1}\mathbf{A}^T}\,\left(\frac{m}{p}\right)\right]\frac{\sigma_m}{m} \qquad (43)
\end{aligned}
$$

The quantity within the square braces of Eq. (43) represents the noise gain for the parameter estimator based on DDTV measurements. The precision in the parameter estimate relative to the parameter value is the product of this noise gain and the relative noise-induced error in the measurement.

Recall that m and p are appropriately-weighting integrals of C_n^2 over the propagation path. These integrals may be substituted into Eq. (43) to yield:

$$\frac{\sigma_{\hat{p}}}{p} = \left[\sqrt{\mathbf{A}\,(\mathbf{P}^T\mathbf{P})^{-1}\mathbf{A}^T} \left(\frac{\int_0^1 \mathrm{d}\xi\, C_n^2(\xi L)\, w_m(\xi)}{\int_0^1 \mathrm{d}\xi\, C_n^2(\xi L)\, w_p(\xi)} \right) \right] \frac{\sigma_m}{m} \tag{44}$$

We may consider a simple, but non-trivial case of uniform C_n^2 over the propagation path. In this case, we may deduce that:

$$\begin{aligned} \frac{\sigma_{\hat{p}}}{p} &= \left[\sqrt{\mathbf{A}\,(\mathbf{P}^T\mathbf{P})^{-1}\mathbf{A}^T} \left(\frac{C_n^2 \int_0^1 \mathrm{d}\xi\, w_m(\xi)}{C_n^2 \int_0^1 \mathrm{d}\xi\, w_p(\xi)} \right) \right] \frac{\sigma_m}{m} \\ &= \sqrt{\mathbf{A}\,(\mathbf{P}^T\mathbf{P})^{-1}\mathbf{A}^T}\ \frac{\sigma_m}{m}, \end{aligned} \tag{45}$$

where the second step follows from the fact that the weighting functions w_m and w_p are normalized. In this case, we may define a noise gain G_p for the parameter p that is related to the matrix $\mathbf{A}$ for the parameter and the matrix $\mathbf{P}$ for the reconstructor as:

$$G_p = \sqrt{\mathbf{A}\,(\mathbf{P}^T\mathbf{P})^{-1}\mathbf{A}^T}. \tag{46}$$

The noise gain G_p was calculated according to Eq. (46) for each of the atmospheric parameters using the profile reconstructor discussed in Subsection 3.2. These values of G_p are shown in Table 3. These results illustrate that the noise gain for estimating atmospheric parameters using the profile reconstructor is quite low. For instance, with a measurement relative error of 10%, the relative error in the estimate is approximately 1%.

parameter value	relates to	G_p
$8.052\left(\frac{2\pi}{\lambda}\right)^{-7/6} L^{-11/6}\,\mathcal{R}$	Rytov parameter	0.1101
$6.305\left(\frac{2\pi}{\lambda}\right)^{-2} L^{-1}\,{r_0}^{-5/3}$	Fried parameter	0.1538
$0.916\left(\frac{2\pi}{\lambda}\right)^{-2} L^{-8/3}\,{\theta_0}^{-5/3}$	isoplanatic angle	0.1538
m_0	integrated turbulence	0.1163

Table 3: Noise gain for estimating each atmospheric parameter using the apparatus and reconstructor detailed in Subsection 3.2.

4 CONCLUSION

Irradiance-based techniques for C_n^2 profiling using integrated-path measurements are limited by saturation effects and the lack of sound theoretical constructs for analysis. To avoid these difficulties, a technique for profiling C_n^2 values along a propagation path using differential-tilt measurements has been proposed. This technique makes use of relatively simple instrumentation to obtain an ensemble of tilt data. The tilt data is then processed to estimate quantities referred to as the difference of differential-tilt variance or DDTV. The DDTV quantities are unaffected by gimbal motion and additive noise sources. Furthermore, the DDTV quantities each represent a particular weighted integral of C_n^2 over the propagation path. Using the theoretical weighting function for the DDTV measurements, a reconstructor matrix can be derived to obtain C_n^2 estimates over the propagation path.

A system consisting of 2 receive apertures and 3 point sources on each end of the path was considered in this analysis. With this configuration, there are a total of 90 DDTV measurements (45 from each end) with unique path-weighting functions which can be computed from the tilt data. The resulting profile reconstructor was tested against an ensemble of 1000 random profiles. Computed moments from each profile were used as input to the reconstructor with the output being a vector of C_n^2 values. This analysis indicates that the mean relative error in the turbulence strength estimate is approximately 5%. When key atmospheric parameters are computed from the reconstructed profiles, the relative error in the Fried parameter and isoplanatic angle is less than 2%. The relative error in the Rytov parameter and mean turbulence strength is approximately 3%. The noise gain for estimating any of these parameters is less than 0.2, indicating that the precision of the estimator is not adversely affected by residual noise contributions.

5 REFERENCES

[1] M. C. Roggemann, B. M. Welsh, and R. Q. Fugate, "Improving the resolution of ground-based telescopes," *Rev. Mod. Phys.* **69**, pp. 437–505, April 1997.

[2] D. C. Washburn *et al.*, "Airborne Laser Extended Atmospheric Characterization Experiment (ABLACE)," Tech. Rep. PL-TR–96-1084, Phillips Laboratory, Kirtland Air Force Base, New Mexico, 1996.

[3] M. R. Whiteley *et al.*, "Airborne Laser Advanced Concepts Testbed Dynamic Compensation Experiment (DyCE)," tech. rep., Air Force Research Laboratory Directed Energy Directorate, Kirtland Air Force Base, New Mexico, 2000.

[4] D. L. Fried, "Optical resolution through a randomly inhomogeneous medium for very long and very short exposures," *J. Opt. Soc. Am.* **56**, pp. 1372–1379, October 1966.

[5] C. A. Primmerman, T. R. Price, R. A. Humphreys, B. G. Zollars, H. T. Barclay, and J. Herrmann, "Atmospheric-compensation experiments in strong-scintillation conditions," *Applied Optics* **34**, pp. 2081–2088, April 1995.

[6] D. L. Fried, "Anisoplanatism in adaptive optics," *J. Opt. Soc. Am.* **72**, pp. 52–61, January 1982.

[7] F. D. Eaton, S. A. McLaughlin, and J. R. Hines, "A new frequency-modulated continuous wave radar for studying planetary boundary layer morphology," *Radio Science* **30**, pp. 75–88, January 1995.

[8] G. D. Nastrom and F. D. Eaton, "Variations of winds and turbulence seen by the 50-MHz radar at White Sands Missile Range, New Mexico," *Journal of Applied Meteorology* **34**, pp. 2135–2148, October 1995.

[9] F. D. Eaton and G. D. Nastrom, "Preliminary estimates of the vertical profiles of inner and outer scales from White Sands Missile Range, New Mexico VHF radar observations," *Radio Science* **33**, pp. 895–903, July 1998.

[10] V. A. Kluckers, N. J. Wooder, T. W. Nicholls, M. J. Adcock, I. Munro, and J. C. Dainty, "Profiling of atmospheric turbulence strength and velocity using a generalised SCIDAR technique," *Astronomy and Astrophysics* **335**(1), 1998.

[11] C. R. Neyman and B. E. Stribling, "Scintillation detection and ranging (SCIDAR) at the air force maui optical station," in *Proc. SPIE: Propagation and Imaging through the atmosphere*, M. C. Roggemann and L. R. Bissonnette, eds., vol. 3763, pp. 259–267, 1999.

[12] M. R. Whiteley, "Rytov parameter estimation by use of differential-tilt measurements," in *Proc. SPIE: Propagation and Imaging IV*, M. C. Roggemann, ed., vol. 4125, p. in press, 2000.

[13] L. C. Andrews, R. L. Phillips, C. Y. Hopen, and M. A. Al-Habash, "Theory of optical scintillation," *J. Opt. Soc. Am. A* **16**, pp. 1417–1429, June 1999.

[14] D. L. Fried, "Differential angle of arrival: Theory, evaluation, and measurement feasibility," *Radio Science* **10**, pp. 71–76, January 1975.

[15] F. D. Eaton, W. A. Peterson, J. R. Hines, J. J. Drexler, A. H. Waldie, and D. B. Soules, "Comparion of two techniques for determining atmospheric seeing," in *Proc. SPIE: Optical, Infrared, and Millimeter Wave Propagation Engineering*, vol. 926, pp. 319–334, 1988.

[16] F. D. Eaton, W. A. Peterson, and J. R. Hines, "Phase structure function measurements with multiple apertures," in *Proc. SPIE: Propagation Engineering*, vol. 1115, pp. 218–223, 1989.

[17] M. R. Whiteley, *Optimal atmospheric compensation for anisoplanatism in adaptive-optical systems*. PhD thesis, Air Force Institute of Technology, Wright-Patterson Air Force Base, Ohio, 1998.

[18] M. R. Whiteley, M. C. Roggemann, and B. M. Welsh, "Temporal properties of the Zernike expansion coefficients of turbulence-induced phase aberrations for aperture and source motion," *J. Opt. Soc. Am. A* **15**, pp. 993–1005, April 1998.

[19] M. R. Whiteley, B. M. Welsh, and M. C. Roggemann, "Optimal modal wave-front compensation for anisoplanatism in adaptive optics," *J. Opt. Soc. Am. A* **15**, pp. 2097–2106, August 1998.

[20] S. M. Kay, *Fundamentals of Statistical Signal Processing: Estimation Theory*, Prentice-Hall, Upper Saddle River, NJ, 1993.

[21] G. Strang, *Linear Algebra and its Applications*, Harcourt Brace Jovanovich, Fort Worth, third ed., 1988.